



HAL
open science

RED GIANT STARS: FROM MIXED MODES TO ANGULAR MOMENTUM

K. Belkacem

► **To cite this version:**

K. Belkacem. RED GIANT STARS: FROM MIXED MODES TO ANGULAR MOMENTUM. EAS Publications Series, 2019, 82, pp.189-211. 10.1051/eas/1982019 . hal-02335186

HAL Id: hal-02335186

<https://hal.science/hal-02335186>

Submitted on 28 Oct 2019

HAL is a multi-disciplinary open access archive for the deposit and dissemination of scientific research documents, whether they are published or not. The documents may come from teaching and research institutions in France or abroad, or from public or private research centers.

L'archive ouverte pluridisciplinaire **HAL**, est destinée au dépôt et à la diffusion de documents scientifiques de niveau recherche, publiés ou non, émanant des établissements d'enseignement et de recherche français ou étrangers, des laboratoires publics ou privés.

RED GIANT STARS: FROM MIXED MODES TO ANGULAR MOMENTUM

K. Belkacem¹

Abstract. Solar-like oscillations are ubiquitous to low-mass stars from the main-sequence to the red-giant branch as demonstrated by the space-borne missions CoRoT and *Kepler*. Understanding the physical mechanisms governing their amplitudes as well as their behavior along with the star evolution is a prerequisite for interpreting the wealth of seismic data and for inferring stellar internal structure. In this paper, I discuss our current knowledge of mode amplitudes with particular emphasis on non-radial modes in red giants (hereafter mixed modes). Then, I will show how these modes permit to unveil the rotation of the inner-most layers of low-mass stars and how they put stringent constraints on the redistribution of angular momentum.

1 Introduction: Mixed modes as a cornerstone for unveiling the core of red giants

Low-mass main-sequence stars with an extended external convective region exhibit acoustic standing waves (hereafter p -modes). Those modes, with high amplitudes near the surface, mainly probe the external layers of these stars. It thus allows us to perform stellar seismology as was successfully done using the CoRoT (*e.g.*, Grotsch-Noels & Deheuvels 2016) and *Kepler* (*e.g.*, Chaplin & Miglio 2013) observations. In contrast, g -modes, whose restoring force is buoyancy, are potentially able to probe the innermost layers of stars. They have relatively low frequencies and very low amplitudes at the stars surface because they are evanescent in the outer convective region (*e.g.*, Belkacem *et al.* 2009). However, except for the Sun for which the detection remains controversial (*e.g.*, Appourchaux *et al.* 2010), those modes have not (yet) been detected in solar-like stars.

For evolved stars, the situation is more favourable. Indeed, while initially thought as complex, oscillation spectra of subgiants and redgiants have proven to

¹ LESIA, Observatoire de Paris, CNRS, PSL Research University, Université Pierre et Marie Curie, Université Denis Diderot, 92195 Meudon, France

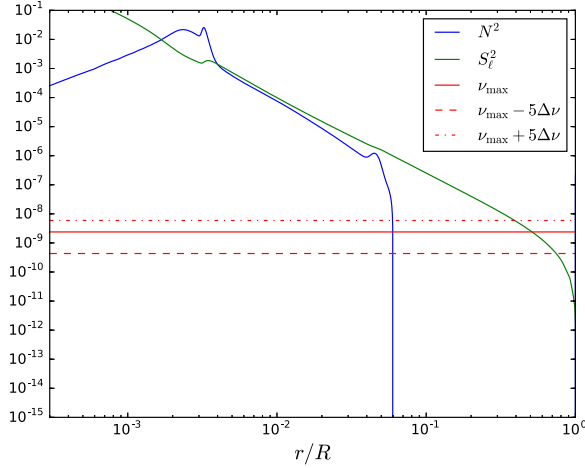


Fig. 1. Propagation diagram showing the squared buoyancy frequency (N^2), the squared Lamb frequency for dipolar modes ($S_{\ell=1}^2$) versus the normalized radius. The solid red line corresponds to the squared ν_{\max} frequency computed using the now classical scaling relation (e.g. Belkacem *et al.* 2011) and the dashed and dashed-dotted red lines correspond to the typical frequency range in which modes are detected. The equilibrium model correspond to an evolved red giant (RGB) stars (and more precisely to model M2 in Belkacem *et al.* 2015a).

be a rich harvest of information on the innermost layers of these stars. This was made possible thanks to space-borne missions and the first detection by CoRoT of thousands of oscillating redgiant stars (see Mosser & Miglio 2016, for a review on early results obtained by CoRoT). Those stars exhibit solar-like oscillations with high amplitudes and more importantly non-radial oscillations later identified as mixed modes (e.g., De Ridder *et al.* 2009). Indeed, a star leaving the main-sequence experiences major structural changes since its radiative core contracts as the result of which its envelope expands. As the total radius increases, both the mean density and the surface gravity decrease. It results in a situation for which a p -mode (for a given radial order and angular degree) is found at a lower frequency as does the frequency of the maximum in the power spectrum (as it scales predominantly with the surface gravity, see Belkacem *et al.* 2011, for details). In contrast, the frequencies of g modes increase because the core contracts while the star evolves. This is due to the increase of the buoyancy frequency. This results in an overlap of the frequency ranges of p and g modes and allow for the appearance of the so-called *mixed-modes* (e.g., Dziembowski *et al.* 2001; Dupret *et al.* 2009). The resonant cavities are depicted by Figure 1.

These modes have a dual nature because they propagate both in the outer and inner cavities. This is a key advantage because they have amplitude at the surface so that it is possible to detect them and bear information on the innermost regions

of the star. Obviously, depending on frequency, each mixed mode bears a different information. At first order, it is possible to define and characterize the *degree of mixity* of a mode by introducing the normalized mode energy, *i.e.*

$$E = \int_0^1 \epsilon \, dx \quad \text{with} \quad \epsilon = \frac{1}{\xi_r(R)^2} (\xi_r^2 + \Lambda \xi_h^2) \quad (1.1)$$

where ξ_r, ξ_h are the radial and horizontal components for the eigenfunction, $\Lambda = \ell(\ell + 1)$ with ℓ the angular degree, $x = m/M$, and M, R the total mass and radius respectively. The normalized mode energy given by Equation (1.1) is plotted in Figure 2 (middle panel). For non-radial modes, the normalized mode energy varies with frequency and is found always higher than for radial modes. It allow us to define p and g -dominated modes that bear a different information. Indeed, p -dominated modes have a low energy and mainly probe the upper layers while the g -dominated modes have a high energy and mostly probe the inner-most regions as shown by Figure 2 (bottom panel).

At the time of the first detection and identification of non-radial modes by CoRoT (De Ridder *et al.* 2009), most of the theoretical background was already developed for decades. These *mixed modes*, as named in the early works of Dziembowski (1971) for Cepheids and Scuflaire (1974) for a condensed polytropic model, have been subject to an extensive investigation from a theoretical point of view (*e.g.*, Shibahashi 1979; Dziembowski *et al.* 2001; Christensen-Dalsgaard 2004). Consequently, the foundations being established, the wealth of observations as provided by CoRoT and followed by *Kepler* gave us the opportunity of a new grip on stellar physics of advanced evolutionary stages.

Nevertheless, a number of fundamental questions were still to be solved. The first crucial issue was the mixed modes detectability and this is addressed in Section 2. Before using those modes for doing seismology and inferring the innermost structure of evolved stars, it was mandatory to be able to identify them and thus to understand the evolution of their amplitude versus the duration of the observations and across the Hertzsprung-Russell diagram. Subsequently, as discussed in Section 3, once mode frequencies are extracted, one must be able to disentangle between several physical effects affecting them such as the glitches, the effect of mode trapping, as well as rotation. Given the complexity of oscillation spectra of evolved stars, this was a crucial prerequisite to be able to properly infer the structure of those stars. Eventually, the mean core rotation of a cohort of evolved stars being inferred, it was possible to emphasize our deficient knowledge about the redistribution of angular momentum in low-mass evolved stars. As we will discuss in Section 4, a number of physical mechanisms are suspected to operate but the picture is far from being grasped and it will certainly give grounds for a harvest of theoretical works in the forthcoming years.

2 Mixed modes detectability

For using mixed modes as probes of the internal structure of stars, it is fundamental to understand the physics governing mode amplitudes. Indeed, this knowledge is

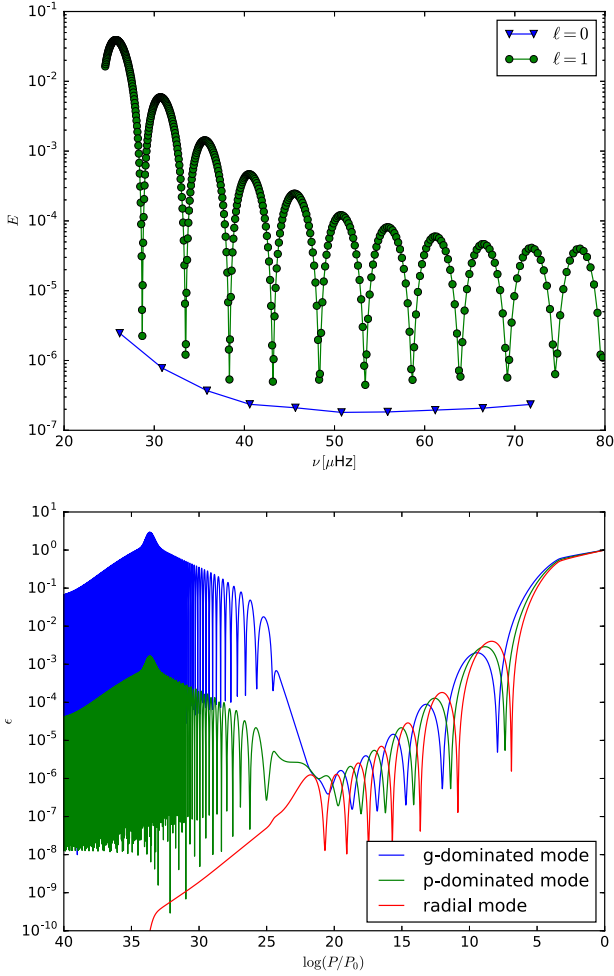


Fig. 2. *Top panel:* Normalized mode energy computed using Equation (1.1) as a function of the frequency for radial and dipolar modes. *Bottom panel:* Integrand of the mode energy ϵ (see Eq. (1.1)) versus the logarithm of the pressure where P_0 is the pressure at the surface.

mandatory to understand the structure of oscillation spectra. Mode amplitudes in evolved stars is however a long-standing and still not completely solved issue (see the review by Samadi *et al.* 2015). The problem can be split into two separate sub-problems, namely; the amplitude of radial modes and the amplitude of non-radial (or mixed) modes.

2.1 Radial mode amplitude for evolved stars

In this section we consider the amplitudes of radial modes in terms of both surface velocity and intensity fluctuations. Based on our knowledge of the solar

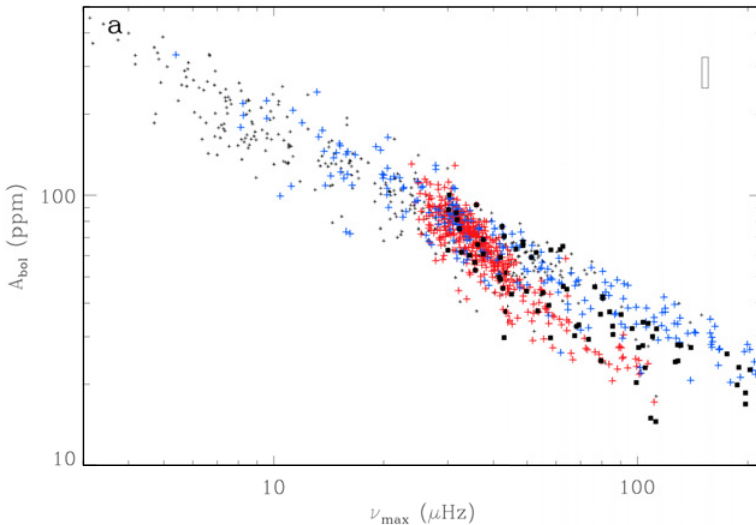


Fig. 3. Maximum height in the power spectrum (at $\nu = \nu_{\max}$) for stars observed by *Kepler*. The color code indicates the evolutionary status; clump stars in red, giant branch stars in blue, unknown status in dark grey. The black squares indicate low-amplitude dipolar modes (see Mosser *et al.* 2017, for details on those particular stars). From Mosser *et al.* (2012a).

oscillations, early attempts have been made to extrapolate the calculations to more evolved stars (*e.g.*, Christensen-Dalsgaard & Frandsen 1983; Kjeldsen & Bedding 1995; Houdek *et al.* 1999; Samadi *et al.* 2007). However, as shown by the space-borne mission (Baudin *et al.* 2011; Mosser *et al.* 2012a) the physical picture is quite different for a red giant compared to the Sun and it needs a particular attention. Indeed, as shown by Figure 3 there is a clear dependence of the maximum height of the power spectrum to the frequency ν_{\max} which is not obvious to reproduce using only our knowledge of mode amplitude in main-sequence stars. This motivated several attempts to reproduce the evolution of mode amplitudes across the HR diagram using empirical scaling relations (*e.g.*, Kjeldsen & Bedding 2011; Huber *et al.* 2011; Corsaro *et al.* 2013) as well as theoretical studies (Samadi *et al.* 2012).

To gain knowledge on mode amplitudes in red giants, the first step consisted in considering radial mode amplitudes. To do so, let us first recall that the mean-squared surface velocity of a mode is given by (Samadi 2011)

$$v^2(\nu, r) = \frac{\tau(\nu)}{2} \frac{P(\nu)}{\mathcal{M}(\nu, r)}, \quad (2.1)$$

where ν is the modal frequency, τ is the mode life-time (which is equal to the inverse of the mode damping rate η), r is the radius in the atmosphere at which

the mode velocity is measured, P is the excitation rate, and \mathcal{M} is the mode mass defined by

$$\mathcal{M} = \frac{I}{|\xi_r(R)|^2} = \frac{1}{|\xi_r(R)|^2} \int_0^R (\xi_r^2 + \Lambda \xi_h^2) \rho r^2 dr, \quad (2.2)$$

where ρ is the density, and R is the total radius of the star.

Therefore, to reproduce the scaling relation as shown by Figure 3, one must be able to provide physically-grounded scaling relations for the mode lifetimes, mode excitation rates, and mode masses. This is a non-trivial task since the underlying physics is complex and depends on the still poorly-known upper-most layers of solar-like stars. To cope with this problem, Samadi *et al.* (2012) proposed to use a grid of 3D hydrodynamical simulations to determine scaling relations for both the excitation rates and mode masses at ν_{\max} . For $\tau(\nu_{\max})$, it is also possible to use the relation derived by Belkacem *et al.* (2012). Consequently, the amplitudes can be written such as

$$v_{\max} = v_{\max,\odot} \left(\frac{T_{\text{eff}}}{T_{\text{eff},\odot}} \right)^{-0.75} \left(\frac{\nu_{\max}}{\nu_{\max,\odot}} \right)^{-1.15} \left(\frac{\Delta\nu}{\Delta\nu_{\odot}} \right). \quad (2.3)$$

where T_{eff} is the effective temperature, ν_{\max} the frequency of the maximum height in the oscillation power spectrum, and $\Delta\nu$ the large separation. The symbol \odot denotes the solar reference values. Equation (2.3) then enable us to estimate the variation of mode amplitude with the evolution of a star when leaving the main-sequence. Indeed, as a star evolves, its surface gravity and effective temperature decrease so that both the large separation and the frequency ν_{\max} significantly decrease. It results in a significant increase of the mode amplitudes, together with a decrease of the mode linewidths, and it explains why so many red giants have been observed with solar-like oscillations.

However, most of the observations are obtained using photometric facilities and mainly with CoRoT and *Kepler* space-scrafts. Therefore, in order to compare predicted and measured mode amplitudes, it is necessary to convert mode-velocity amplitudes to intensity amplitudes and more precisely to luminosity perturbations $\delta L/L$ where $\delta L(t)$ is the mode Lagrangian (bolometric) luminosity perturbations. This is a non-trivial task and a consistent calculation requires to take into account the energy gain/lost by the pulsation. This can be done by using a non-adiabatic pulsation code that takes into account coupling between oscillation, radiation and turbulent convection. Due to the difficulties of consistently treating the underlying mechanisms, the use of the quasi-adiabatic relation has been proposed by Kjeldsen & Bedding (1995) as well as Severino *et al.* (2008). However, those simple estimates fail to reproduce the observations and one needs to abandon the quasi-adiabatic assumption which is not justified in the upper-most layers of red giants. It thus motivated Samadi *et al.* (2012) to use a more sophisticated approach and more precisely the MAD non-adiabatic pulsation code (Grigahcène *et al.* 2005). They established that the ratio between luminosity and velocity scales as the ratio

$(L/M)^\alpha$ with $\alpha = 0.25$ (see Samadi *et al.* 2012, 2015, for details). Using this result, it is quite straightforward to show that

$$\frac{\delta L}{L} \propto T_{\text{eff}}^{0.125} \nu_{\text{max}}^{-0.75}. \quad (2.4)$$

Because we are considering red giant stars, the dependence with the effective temperature in Equation (2.4) is negligible, and we mainly have $\delta L/L \propto \nu_{\text{max}}^{-0.75}$. When compared to the fit on the *Kepler* observations (see Fig. 3) as done by Mosser *et al.* (2012a), the agreement is quite satisfactory. Indeed, Mosser *et al.* (2012a) obtained $\delta L/L \propto \nu_{\text{max}}^{-0.751}$ (see their Table 3). Therefore, one can conclude that the main physics underlying radial mode amplitudes is grasped. However, there are still some discrepancies identified by Samadi *et al.* (2012) to be due to both the conversion between luminosity and velocity amplitudes as well as non-adiabatic effects affecting mode driving.

2.2 Non-radial mode amplitude for evolved stars

Let us now consider the case of non-radial modes. The absolute amplitudes of those modes is subject to the same uncertainties as for radial modes as well as an additional difficulty related to the inner radiative damping. To focus on the latter, we will then consider the ratio between dipolar and radial modes of comparable frequencies. For sake of clarity, we will also consider that all modes are resolved, *i.e.* their lifetimes are smaller than the duration of the observations ($\tau \ll T_{\text{obs}}$). In practise this is not always the case and this introduces additional subtleties but we refer the reader to Dupret *et al.* (2009) and Grosjean *et al.* (2014) for a detailed discussion in this situation.

As shown by Benomar *et al.* (2014), the ratio between mode heights in the power spectrum reads

$$\frac{H_\ell}{H_0} = \left(\frac{P_\ell}{P_0} \right) \left(\frac{\mathcal{M}_0}{\mathcal{M}_\ell} \right) \left(\frac{\eta_0}{\eta_\ell} \right)^2, \quad (2.5)$$

where radial modes ($\ell = 0$) are denoted by the subscript 0, and non-radial modes by the subscript ℓ . In term of mode amplitude, it gives

$$\frac{A_\ell^2}{A_0^2} = \left(\frac{P_\ell}{P_0} \right) \left(\frac{\mathcal{M}_0}{\mathcal{M}_\ell} \right) \left(\frac{\eta_0}{\eta_\ell} \right), \quad (2.6)$$

where the relation between mode amplitude and mode height is $A^2 = H\eta/2$ (see for instance Libbrecht 1988; Baudin *et al.* 2005; Chaplin *et al.* 2005; Belkacem *et al.* 2006). Note that in our notation, the mode amplitude A can be expression in term of both mode velocity or luminosity fluctuations as discussed in Section 2.1.

To go further, we note that at similar frequencies, the eigenfunctions of radial and non-radial modes have similar shapes in the super-adiabatic layers (*i.e.*, near the photosphere). Therefore, the work done by the driving source on the modes is the same. This has been shown by Dupret *et al.* (2009) and Benomar *et al.*

(2014). Obviously, for very low frequencies and high angular degrees, this is no longer verified since the horizontal component of the eigenfunction for non-radial modes become non-negligible. This leads to

$$P_0 \mathcal{M}_0 \simeq P_\ell \mathcal{M}_\ell. \quad (2.7)$$

Finally, using Equation (2.6) together with Equation (2.7), one obtains the desired relation for the mode amplitude ratio

$$\frac{A_\ell^2}{A_0^2} \simeq \left(\frac{\mathcal{M}_0}{\mathcal{M}_\ell} \right)^2 \left(\frac{\eta_0}{\eta_\ell} \right). \quad (2.8)$$

Equation (2.8) is quite enlightening because it explicitly shows that mainly two physical ingredients are susceptible to affect the amplitude of non-radial modes compared to the radial ones, namely; the mode trapping (through the inertia ratio) and an extra-contribution of mode damping. We also note that in all cases¹ one has $A_\ell \leq A_0$. Indeed, if non-radial modes are efficiently trapped in the core or experience a strong damping in the core, their amplitudes will be diminished compared to the radial modes and the question of their detectability is obviously raised.

Actually, in the radiative interiors, the dominant contribution of mode damping is what we call *the radiative damping* since normal modes with a non-negligible amplitude lose energy radiatively. The influence of radiative damping has already been extensively investigated for other classes of pulsators (see Samadi *et al.* 2015, for details) and even before the unambiguous detection by CoRoT of non-radial modes in red giants, this question had been investigated from a theoretical point of view by Dziembowski *et al.* (2001) following the detection of variability in the red giant α UMa by Buzasi *et al.* (2000) using photometric data from the WIRE satellite. Concomitantly with the detection of non-radial stochastically excited modes in red giants by CoRoT (De Ridder *et al.* 2009; Dupret *et al.* 2009) investigated the effect of radiative damping and trapping on the amplitude of non-radial modes along with the evolution of stars with masses of $2 M_\odot$ and $3 M_\odot$. This early work was based on a full computation of mode driving as well as non-adiabatic mode damping and was extensively used to qualitatively understand the oscillation power spectrum observed by CoRoT (see the review by Mosser *et al.* 2016, for an account of the evolution of our understanding of redgiant spectra at the time of the CoRoT mission). This work was supplemented by Grosjean *et al.* (2014) who focused on low-mass red giants as mainly observed by the CoRoT and *Kepler* spacecrafts (see Fig. 4). The main conclusion is that radiative damping becomes dominant either for high-angular degrees or highly evolved red giant stars. In those cases, the non-radial modes can be severely affected and their amplitudes decrease so that they cannot be detected. The main physical

¹ Note that this inequality does not take the visibilities into account.

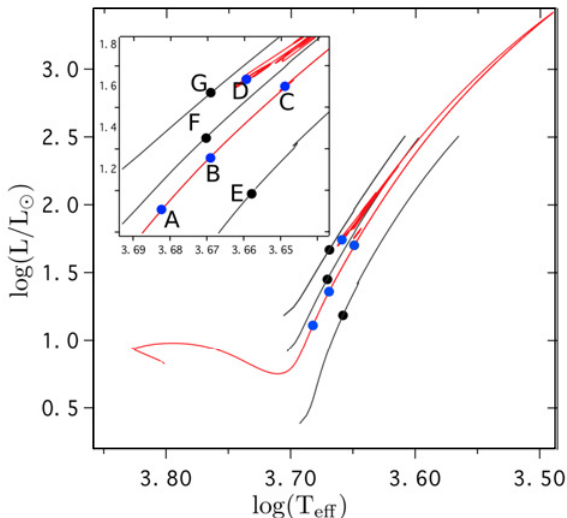


Fig. 4. Hertzsprung-Russel diagram for a $1.5 M_{\odot}$ evolutionary track in red solid line and $1.7, 2 M_{\odot}$ in black. The dots are the selected models by Grosjean *et al.* (2014) for an in-depth study. From Grosjean *et al.* (2014).

ingredient is thus the ratio between the work associated with the damping in the core and in the envelope. To show it, let us remind that $\eta_{\ell} = W_{\ell}/\mathcal{M}_{\ell}$, with W_{ℓ} the total work integral associated to the damping (*e.g.* Belkacem *et al.* 2011), so that Equation (2.8) becomes

$$\frac{A_{\ell}^2}{A_0^2} \simeq \left(\frac{\mathcal{M}_0}{\mathcal{M}_{\ell}} \right) \left(\frac{W_0}{W_{\ell}} \right). \quad (2.9)$$

To go further, it is useful to write $W_{\ell} = W_{\text{env}} + W_{\text{core}}$, where W_{env} and W_{core} are the work integrals associated to the envelope and the core, respectively. Moreover, using the same argument as for the driving (see Eq. (2.7)) one can assume $W_{\text{env}} = W_0$ so that

$$\frac{A_{\ell}^2}{A_0^2} \simeq \left(\frac{\mathcal{M}_0}{\mathcal{M}_{\ell}} \right) \left(1 + \frac{W_{\text{core}}}{W_0} \right)^{-1}. \quad (2.10)$$

The evolution of the ratio W_{core}/W_0 is illustrated by Figure 5 and its influence on the shape of the oscillation power spectra is shown in Figure 6. Guided by the above-mentioned arguments and using complete computations of mode driving and damping, Grosjean *et al.* (2014) were able to theoretically predict the limit of mixed mode detectability commensurable with the observations. The authors also demonstrated that the structure of oscillation spectra is identical for a given ratio of the number of mixed modes between two consecutive p modes (n_g/n_p) as depicted by Figure 7.

Finally, it is worthwhile to note that the amplitude ratio can be easily estimated using asymptotic developments. From Equation (2.10), there are two distinct

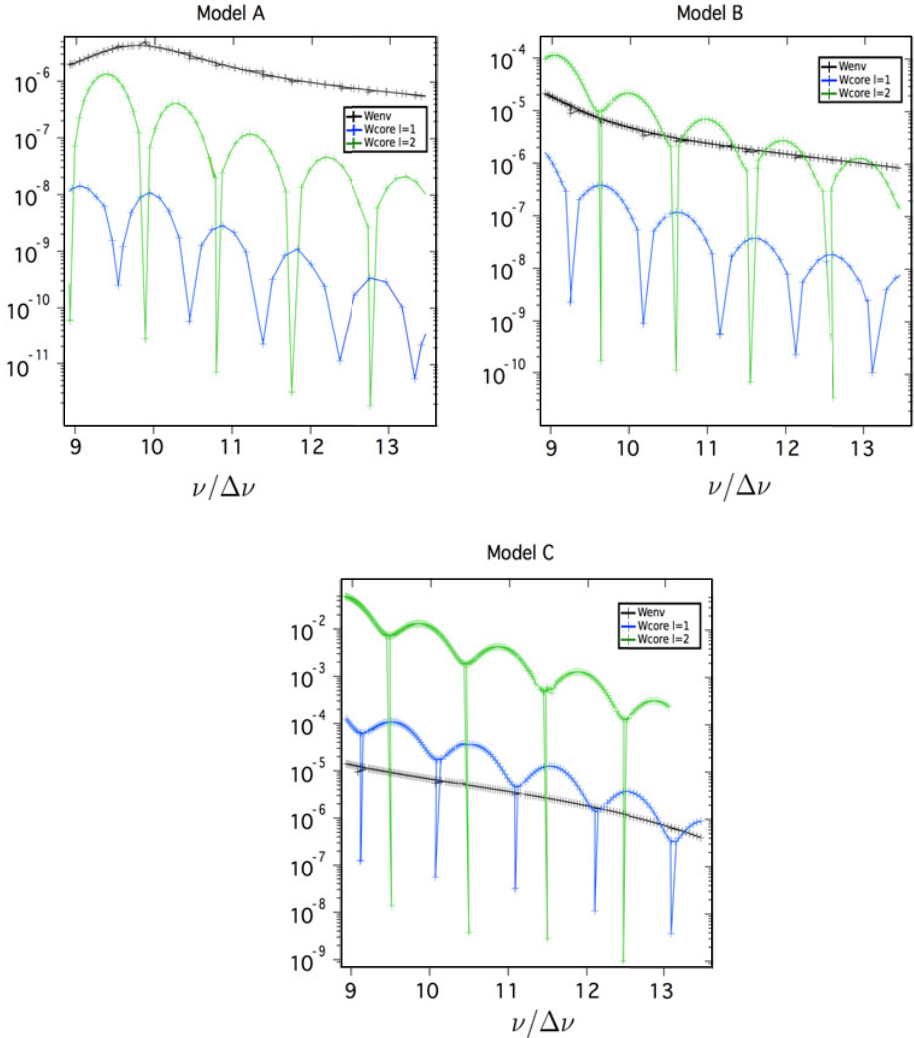


Fig. 5. Core and envelope contributions to the work integral, normalised by GM^2/R , for the three models A,B,C (from top to bottom panels, respectively) of the 1.5 M evolutionary tracks as shown by Figure 4. From Grosjean *et al.* (2014).

cases, namely;

- if the work associated with the radiative damping in the core is negligible compared to the work associated with the damping in the envelope, the mode amplitude ratio Equation (2.10) reads (see also Belkacem *et al.* 2015a)

$$\frac{A_\ell^2}{A_0^2} \simeq \left(\frac{\mathcal{M}_0}{\mathcal{M}_\ell} \right) = 1 - \zeta, \quad (2.11)$$

where we have introduced the now commonly used ζ function (*e.g.* Goupil *et al.* 2013; Mosser *et al.* 2015) that represents the ratio between the mode

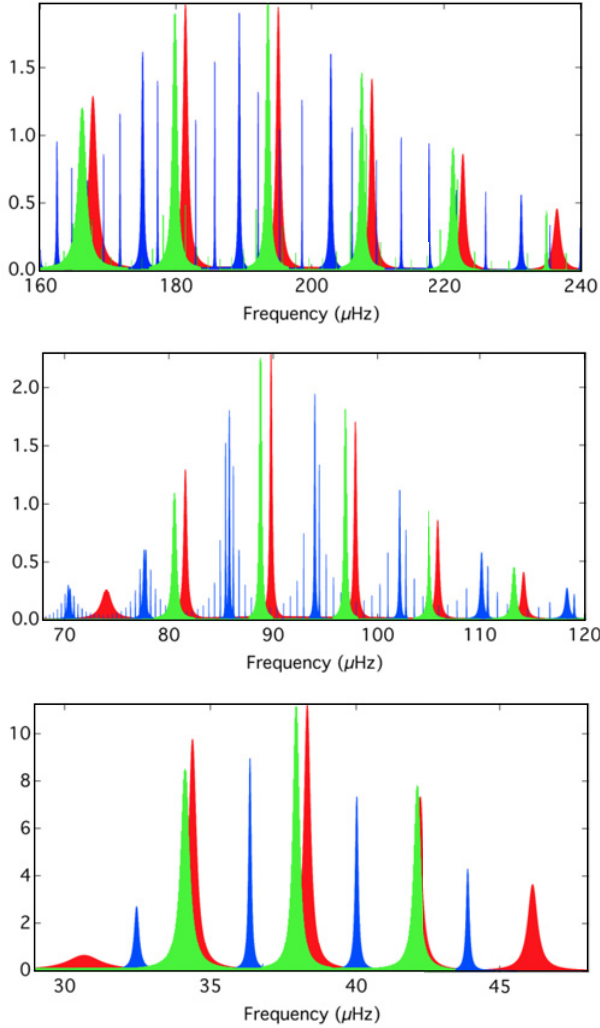


Fig. 6. Power spectra of models A, B, and C (see Fig. 4). The heights are given in $m/s)^2/\mu\text{Hz}$. From Grosjean *et al.* (2014).

inertia in the core and the total mode inertia. As we will show, in the following section, this function can be easily determined using asymptotic developments. Equation (2.11) holds for the low angular degrees in subgiants and early red giants.

- if W_{core} cannot be neglected compared to W_0 one can also estimate the amplitude ratio using asymptotic developments by writing

$$\frac{A_\ell^2}{A_0^2} \simeq \frac{1 - \zeta}{1 + \frac{\eta_{\text{core}}}{\eta_0} \zeta}, \quad (2.12)$$

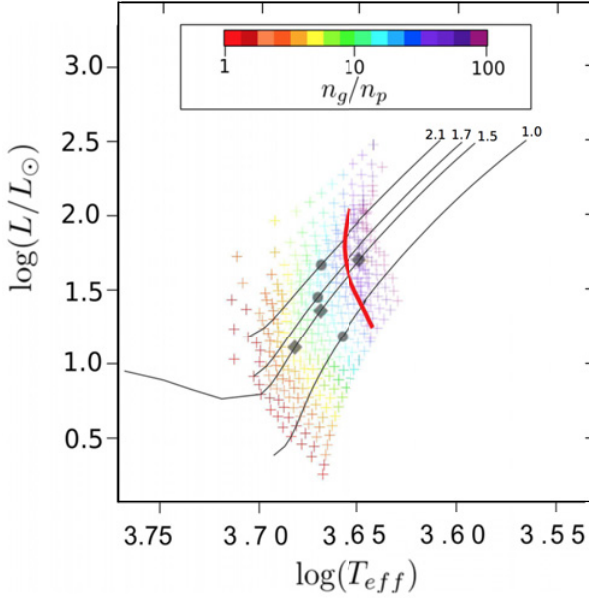


Fig. 7. The same as in Figure 4 except that the color scale indicates models with the same number of mixed modes by large separation. The red line represents the detectability limit found for the dipole modes by Grosjean *et al.* (2014) (assuming that all modes are fully resolved). From Grosjean *et al.* (2014).

where η_0 can be easily determined using observations or scaling relation as for instance given by Belkacem *et al.* (2012), and η_{core} is the radiative damping which can be written as (*e.g.* Dziembowski *et al.* 2001; Godart *et al.* 2009)

$$\eta(\ell_{\text{max}}, \nu) = \frac{[\ell_{\text{max}}(\ell_{\text{max}} + 1)]^{3/2}}{8\pi\sigma_R^3 \int_0^{R_c} k_r dr} \int_0^{R_c} \frac{\nabla_{\text{ad}} - \nabla}{\nabla} \frac{\nabla_{\text{ad}} N g L}{P r^5} dr. \quad (2.13)$$

where $k_r^2 \simeq \frac{\ell(\ell+1)}{r^2} \left(\frac{N^2}{\sigma_R^2} \right)$, N is the buoyancy frequency, P is the pressure, L is the luminosity, R_c is the base of the convective region, $\sigma_R = 2\pi\nu$, ∇ is the temperature gradient and ∇_{ad} its adiabatic counter-part.

Finally, one can conclude that the main physics underlying the oscillation power spectra of evolved stars among the HR diagram is now grasped. It was a crucial and even mandatory step before using the mixed modes for inferring the internal structure of red giants. However, even if the structure and evolution of the spectra is understood, one still must be able to properly know what kind of information bear the oscillation frequencies and this is not a trivial task as shown in the following section.

3 Mixed mode frequencies: Disentangling mode trapping, glitches, and rotational splittings

Once detected, mixed modes are not directly usable to infer the internal structure of evolved stars. Indeed, a number of physical mechanisms influence their frequencies. The main challenge is thus to disentangle all the contributions. This is a non-trivial task and quite a number of studies focused on that objective (see the review by Hekker & Christensen-Dalsgaard 2016) but it is safe to realize that all those works rely directly or implicitly on asymptotic expansions. They allow us to link the frequencies with structural properties of stars in idealized situations. Asymptotic developments are therefore unique and essential tools to gain knowledge on the structure of oscillation spectra.

3.1 Asymptotic expansion for mixed modes

Pure gravity mode frequencies are equally spaced in periods. It is the counterpart of the large separation for pure acoustic modes. Indeed, gravity mode periods follow the relation (Tassoul 1980)

$$\Pi = \Delta\Pi(n + \epsilon_g), \quad (3.1)$$

where ϵ_g is a phase shift, n is the radial order, and $\Delta\Pi$ is the period spacing given by

$$\Delta\Pi = \frac{2\pi^2}{\sqrt{\ell(\ell+1)}} \left(\int_{r_1}^{r_2} N \frac{dr}{r} \right)^{-1}, \quad (3.2)$$

where r_1 and r_2 are the radius of the inner and outer turning points of the g -mode cavity. It is worth to note that the integral in Equation (3.2) is related to the evolutionary state of the star since it provides information on the inner-most layers of evolved stars. For instance, it has been possible to unambiguously distinguish between low-mass stars on the ascending red-giant branch (RGB) and on the central helium burning phase (clump stars) by using the period spacings while it was impossible to conclude only with surface properties such as effective temperature and surface gravities (Bedding *et al.* 2011; Mosser *et al.* 2011). For both RGB and clump stars it is possible to go a step further since the period spacing is very sensitive to the internal structure of the core and thus to the evolutionary stage.

However, if one uses directly the period spacing between two consecutive mixed modes, ΔP , as in Bedding *et al.* (2011) and Mosser *et al.* (2011), the diagnostic remains limited. Actually, the period spacing between two consecutive observed mixed modes does not follow exactly the asymptotic relation as given by Equation (3.2). This is related to the mixed nature of the modes. The observed modes are not *pure* g -modes because they are affected by their acoustic nature in the envelope that induces a departure from Equation (3.2). This is illustrated by Figure 8.

To cope with this issue, Mosser *et al.* (2012a) proposed an asymptotic relation adapted for mixed modes, essentially a matching between asymptotic solution in

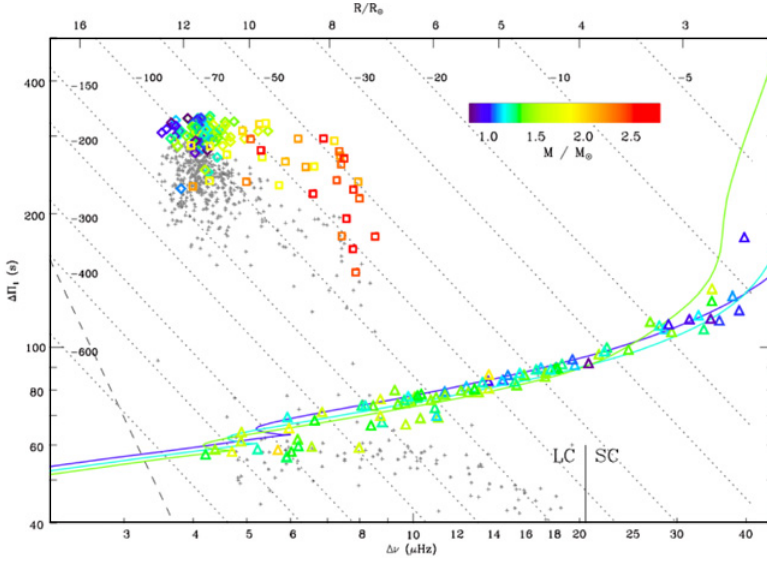


Fig. 8. Gravity-mode period spacing $\Delta\Pi$ as a function of the pressure-mode large frequency spacing $\Delta\nu$. RGB stars are indicated by triangles; clump stars by diamonds; secondary clump stars by squares. The seismic mass is given by the color code. Small gray crosses indicate the bumped periods ΔP . The solid colored lines correspond to a grid of stellar models with masses of 1, 1.2 and 1.4 M_{\odot} , from the ZAMS to the tip of the RGB. From Mosser *et al.* (2012a).

the acoustic and buoyancy cavities (this is based on the original work by Shibahashi 1979b). It allows us to express the mixed mode frequencies as a function of p -mode frequencies, *i.e.*

$$\nu = \nu_{n_p} + \frac{\Delta\nu}{\pi} \arctan \left[q \tan \pi \left(\frac{1}{\Delta\Pi \nu} - \epsilon_g \right) \right], \quad (3.3)$$

where ν is the mixed mode frequency, ν_{n_p} the frequency of *pure* p modes, and q a coupling factor. Therefore, using Equation (3.3) with the measured ν yields a determination of the asymptotic period spacing ($\Delta\Pi$) through a simple fitting. This is a crucial step for comparing the observations and the modelling as well as for determining the evolutionary stage (Mosser *et al.* 2014; Vrad *et al.* 2016). As illustrated by Figure 8, the observed asymptotic period spacing can be easily compared to the period spacing computed by the models using Equation (3.2).

It is possible to go a step further and to relate directly ΔP and $\Delta\Pi$ by considering that it mainly depends on the ratio between the inertia contribution in the g -mode cavity and the total inertia of a mixed mode. More precisely, one has (Christensen-Dalsgaard 2012; Mosser *et al.* 2015)

$$\Delta P = \Delta\Pi \zeta, \quad (3.4)$$

where an asymptotic expression of ζ can be obtained as demonstrated by Goupil *et al.* (2013) and generalized by Deheuvels *et al.* (2015) and Mosser *et al.* (2015), *i.e.*

$$\zeta(\nu) = \left[1 + \frac{1}{q} \frac{\nu^2 \Delta\Pi}{\Delta\nu(\nu_p)} \frac{\cos^2 \frac{\pi}{\Delta\Pi} \left(\frac{1}{\nu} - \frac{1}{\nu_g} \right)}{\cos^2 \pi \frac{\nu - \nu_p}{\Delta\nu(\nu_p)}} \right]^{-1}. \quad (3.5)$$

where ν_p and ν_g are the frequencies of pure p and g modes, respectively.

This ratio is fundamental for understanding mixed mode spectra because, at leading order, it controls almost all the physical parameters such as mode amplitudes (see Sect. 2), period spacing, but also rotational splittings as we will discuss in Section 3.2. Therefore, for inferring precisely the internal structure of red giants, it is essential to remove this dominant dependency. It motivated the work by Mosser *et al.* (2015). The authors proposed an elegant way for extracting higher-order effects from the mixed mode frequencies by introducing a change of variable, named to as *stretched periods*. Assuming that the frequencies and the periods are continuous functions, one can write

$$d\tau = \frac{1}{\zeta} \frac{d\nu}{\nu^2}, \quad (3.6)$$

where τ is the stretched period and ζ is given by Equation (3.5). Figure 9 displays an example for a star observed by *Kepler* in which the rotation is not detected.

3.2 Measurements of core rotation and evidence of spin-down

When rotation is non-negligible, non-antisymmetric modes (*i.e.* with $m \neq 0$, where m is the azimuthal) can be detected albeit it depends on the inclination of the star. Therefore, the frequency difference between the modes with $m = 0$ and $m \neq 0$ can be measured. These are the rotational splittings, $\delta\nu$ (see Goupil 2011 for a review on the influence of rotation on mode frequencies). In red giants, the frequency dependence of the splittings with the frequency is intimately intertwined with the frequency dependence of ΔP . To disentangle between the effects of the trapping (through ζ) and the rotation, the stretched periods are again very useful. If one defines $\delta\tau$ as the difference between the stretched periods of two modes of consecutive radial orders and the same azimuthal order, one has (Mosser *et al.* 2015)

$$\delta\tau = \Delta\Pi + \frac{2m\delta\nu}{\nu} \Delta P = \Delta\Pi \left(1 + \frac{2m\delta\nu}{\nu} \zeta \right). \quad (3.7)$$

Note that Equation (3.7) has been derived assuming the rotation of the envelope can be neglected. This is quite a safe assumption for RGB stars and particularly for g -dominated modes. Equation (3.7) immediately shows that an échelle diagram using the stretched period modulo $\Delta\Pi$ immediately exhibits the rotational splittings as illustrated by Figure 10.

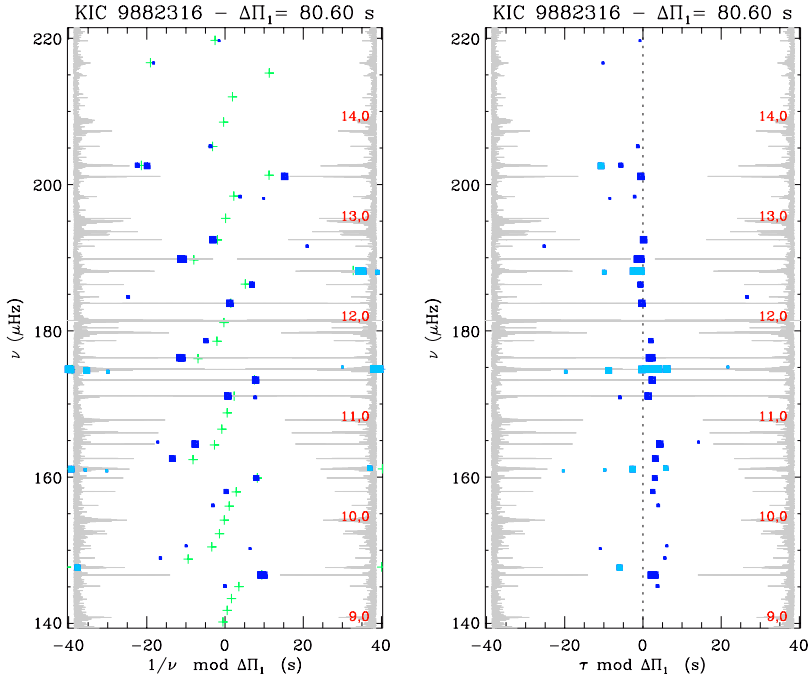


Fig. 9. Échelle diagrams of the RGB star KIC 9882316. The *left panel* shows the classical period chelle diagram, where the abscissa is the period modulo the period spacing. The most prominent mixed modes are marked with blue filled squares (in light blue for peaks in the vicinity of p -dominated modes). The *right panel* displays the stretched period chelle diagram, where the abscissa is the stretched period modulo the period spacing. Pressure-dominated mixed modes are coded in light blue. From Mosser *et al.* (2015).

One must now relate the rotational splittings ($\delta\nu$) and the mean rotation of the core. As above-mentioned and demonstrated by Goupil *et al.* (2013) in the case of linear splitting (see Ouazzani *et al.* 2013 when rotation can no longer be treated as a perturbation), the ratio ζ is still an important factor and one has for g -dominated modes

$$\delta\nu \simeq \frac{1}{2} \left\langle \frac{\Omega}{2\pi} \right\rangle_{\text{core}} \zeta, \quad (3.8)$$

where Ω is the rotational angular frequency. Before going further, it is fundamental to stress out that the symbol $\langle \rangle_{\text{core}}$ denotes the seismic average and must not be directly compared to the core rotation rate inferred in models as unfortunately done in several works. Indeed, one has

$$\left\langle \frac{\Omega}{2\pi} \right\rangle_{\text{core}} = \frac{1}{2\pi} \left(\int_0^{x_{\text{core}}} \Omega(x) K(x) dx \right) \left(\int_0^{x_{\text{core}}} K(x) dx \right)^{-1}, \quad (3.9)$$

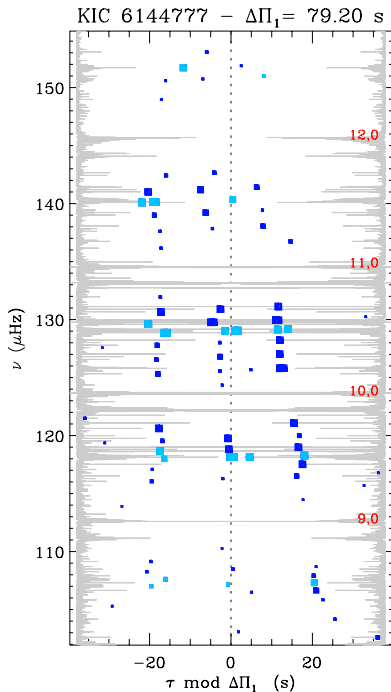


Fig. 10. The same as for Figure 9 but for the star KIC 6144777. The three main ridges are due to the dipolar modes and more precisely to the $m = -1, 0, 1$ modes. From Mosser *et al.* (2015).

with x_{core} the normalized radius of the upper turning point of the g modes which can be approximated by the normalized radius of the radiative core, and

$$K(x) = \frac{1}{I} (\xi_r^2 + (\Lambda - 1)\xi_h^2 - 2\xi_r\xi_h) \rho x^2, \quad (3.10)$$

where I the mode inertia.

Using first-order asymptotic developments as well as numerical calculation, Goupil *et al.* (2013) have shown that this seismic average can be approximated by

$$\left\langle \frac{\Omega}{2\pi} \right\rangle_{\text{core}} \simeq \frac{1}{\tau_g} \int_0^{x_{\text{core}}} \frac{\Omega(x) N}{2\pi x} dx, \quad (3.11)$$

where N is the buoyancy frequency and τ_g is the time spent in the g -mode cavity by a mode defined by

$$\tau_g = \int_0^{x_{\text{core}}} N \frac{dx}{x}. \quad (3.12)$$

Therefore, one must be cautious when comparing seismic core rotation of evolved stars with rotation rates derived from evolutionary models because, as shown by

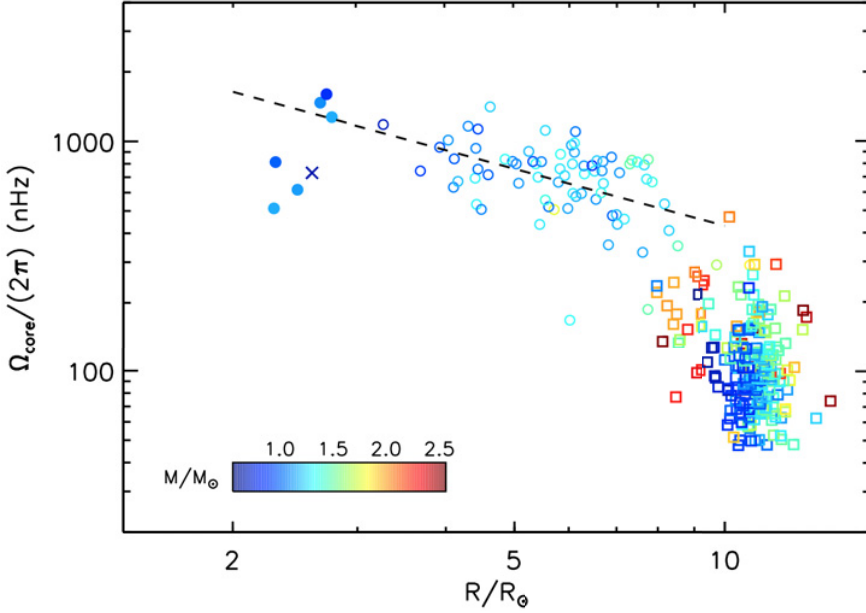


Fig. 11. Rotation rate of the core as a function of the stellar radius. The open dots and open squares correspond to the RGB and clump stars, respectively, investigated by Mosser *et al.* (2012b). The filled symbols indicate the subgiant stars studied by Deheuvels *et al.* (2012, 2014). Figure from Deheuvels *et al.* (2015).

Equation (3.11), the seismic average crucially depends on the rotation profile and how it compares with the buoyancy frequency profile. Moreover, it allows ones to see that the seismic average probes the rotation rate in the inner most layers where N is important. Indeed, it is of no help for the rotation rate in-between the hydrogen burning shell and the base of the upper convective zone.

Such a methodology has been used by Mosser *et al.* (2012b) to infer core rotation of hundreds of RGB and clump stars. For less-evolved stars, namely subgiant stars, Deheuvels *et al.* (2012, 2014) used a different methodology by using inversion techniques. It was made possible mainly because the reciprocal influence of the p and g cavities are less severe so that the information is less degenerated than for more evolved RGB stars. The overall result is well illustrated by Figure 11. Since the total radius is a proxy of the evolutionary stage, one can draw several conclusions, namely

- For subgiant stars, even if the number of stars remains limited, it seems that the radiative core spins-up as expected by considering the local conservation of angular momentum (hereafter AM). Indeed, when a star evolves off-main-sequence, its core contracts. However, anticipating on the following section, the spin-up is not high enough to be compatible with the local conservation

of AM. It means that angular momentum transport is needed to explain the observation.

- For red giant stars, the situation is even more critical since their core spin-down along with their evolution. It is the signature of a powerful physical mechanism able to redistribute AM from the core to the envelope.
- The edge between subgiants and redgiants clearly raises a number of questions. Does the slope change results from a different physical mechanism of AM transport at work and does it simply comes from a difference in the efficiency of a single physical process? The lack of observational data clearly amplifies the questioning but we need to rely on modelling before space-borne missions such as PLATO (Rauer *et al.* 2014) would be able to conclude.

Finally, we can draw a relatively simple conclusion. One or several physical processes must be invoked to explained the efficient angular momentum transport from the core to the envelope of evolved stars.

4 The aftermath: The quest for angular momentum transport

With the measurement of the core rotation of evolved stars it was soon realized that current models including angular momentum redistribution processes are unable to explain the spin-down of red giant stars. Eggenberger *et al.* (2012) investigated the particular case of the star KIC8366239 observed by *Kepler* and tried to reproduce the rotational splittings as measured by Beck *et al.* (2012). Within the approximation of shellular rotation (Zahn 1992), the authors included the angular momentum advection by meridional circulation as well as diffusion of AM by shear mixing and showed that using classical values for turbulent viscosities is not sufficient. This was independently confirmed by Marques *et al.* (2013) (see also Ceillier *et al.* 2013) who showed that even by accounting for the large uncertainties related to the horizontal viscosities as well as to the surface braking law meridional circulation and shear instabilities are unable to explain the low rotation rates of subgiants and red giants. Note, however, that the issue is not completely settled because the the horizontal diffusion coefficient is still subject to discussion (see L. Amard in this Volume). Eggenberger *et al.* (2012) also proposed to constrain the unknown additional mechanism by fitting the turbulent viscosity. This has been generalized by Eggenberger *et al.* (2017) who showed that the efficiency of the missing mechanism increases with the stellar mass. We note, however, that such an approach, while putting stringent constraint on the AM transport, assumes that the additional mechanism is a diffusion process.

Meridional circulation and shear instabilities being helpless for explaining the observations, the potential contribution of the magnetic field was soon to be addressed. Cantiello *et al.* (2014) investigated the effect of a magnetic field generated through the Tayler-Spruit dynamo (see the seminal papers by Spruit 1999, 2002) and reached almost the same negative conclusion. An alternative mechanism,

involving magnetic field, was proposed by Rüdiger *et al.* (2015). The authors investigated the effect of the magneto-rotational instabilities of a toroidal magnetic field (AMRI). They suggest that it could explain the angular momentum redistribution in subgiants and early red giants (see also Maeder & Meynet 2014). Even if their modelling is idealized, for instance assuming chemically homogeneous fluid, the transport of AM by an azimuthal magneto-rotational instability as proposed by Rüdiger *et al.* (2015) constitutes a promising candidate to further investigate. Interestingly enough, Spada *et al.* (2016) fitted to the observations a power law (of the ratio between the rotation frequency of the radiative and convective layers) for the AM diffusion coefficient and showed that the power is compatible with the AMRI.

A second class of non-standard physical process can help in solving the problem of the rotation of evolved stars, namely; waves. This includes both progressive (hereafter mentioned as waves) and standing waves (hereafter mentioned as modes). The former, and mainly internal gravity waves (IGW) can transport angular momentum (*e.g.*, Press 1981) and it has been demonstrated that they could explain the nearly flat rotation profile in the inner radiative zone of the Sun (Charbonnel & Talon 2005). For evolved stars, Fuller *et al.* (2014) have found that internal gravity waves are likely to couple the convective region and the upper radiative region, but not the innermost layers, *i.e.* the core of redgiants. More precisely, they demonstrated that IGW could not reach the core of RGB stars because they are highly damped near hydrogen burning shell (*i.e.* near the peak of the buoyancy frequency). We note however, that it also means a strong local extraction of AM which can potentially have non-negligible influence on other processes such as meridional circulation. This interaction as well as many others remain a weak point in current modelling of angular momentum transport and would deserve attention in the future. In contrast, for subgiants and early redgiants, the recent work by Pinçon *et al.* (2016b) provides new insight on the role of IGW. Based on the formalism developed by Pinçon *et al.* (2016a) to model excitation of IGW by convective plumes, the authors suggest that IGW could explain the observed differential rotation of subgiants and early red giants as observed by Deheuvels *et al.* (2014).

However, for more evolved red giants, IGW are helpless but mixed modes can be decisive. Indeed, mixed modes allowed us to unveil the internal rotation of evolved stars but they can also play an active role. Actually, redistribution of angular momentum by normal modes has been considered for a long time with the pioneer work by Ando (1983) who addressed the question of the interaction of wave and rotation through wave momentum stresses in the mean angular momentum equation, and many works followed in the context of massive stars (*e.g.*, Ando 1986; Lee & Saio 1993; Lee 2007; Townsend & MacDonald 2008; Townsend 2014; Lee *et al.* 2014). To estimate the influence of mixed modes in low-mass evolved stars, Belkacem *et al.* (2015a, 2015b) revisited the formalism to account properly for the influence of both the wave momentum and heat fluxes on the mean flow. Then, using realistic estimates of mode amplitudes, they were able to show that mixed modes are able to efficiently slow-down RGB stars but not subgiants. Thus,

one can conclude that the combination of IGW for sugiants and mixed modes for RGB stars is a competitive candidate to account for the observations. No doubts this will be further investigated in the near future to reach a definitive conclusion.

5 Concluding remarks

Finally, since the unambiguous detection of mixed modes in red giants by CoRoT (De Ridder *et al.* 2009), huge efforts have been made to unveil the interior structure and rotation of these stars. They were highly successful and we can bet that we are only at the beginning of the story. The analysis of existing observational data are still ongoing and the forthcoming grounded-based, such as SONG facility (Grundahl *et al.* 2006), and space-borne missions, such as TESS (Ricker *et al.* 2015) and PLATO (Rauer *et al.* 2014), will certainly be decisive to grasp to physics of angular momentum transport in low-mass stars. Jean-Paul Zahn has always been at the forefront in this topic and no doubt much of the recent advances would have not been made possible without his precursor contributions.

K. B. is grateful to the organizers for their invitation. The author also thanks B. Mosser and R. Samadi for reading the manuscript and for providing useful remarks.

References

- Ando, H., 1983, PASJ, 35, 343
Ando, H., 1986, A&A, 163, 97
Appourchaux, T., Belkacem, K., Broomhall, A.-M., *et al.*, 2010, A&A Rev., 18, 197
Baudin, F., Barban, C., Belkacem, K., *et al.*, 2011, A&A, 529, A84
Baudin, F., Samadi, R., Goupil, M.-J., *et al.*, 2005, A&A, 433, 349
Beck, P.G., Montalbán, J., Kallinger, T., *et al.*, 2012, Nature, 481, 55
Bedding, T.R., Mosser, B., Huber, D., *et al.*, 2011, Nature, 471, 608
Belkacem, K., Dupret, M.A., Baudin, F., *et al.*, 2012, A&A, 540, L7
Belkacem, K., Goupil, M.J., Dupret, M.A., *et al.*, 2011, A&A, 530, A142
Belkacem, K., Marques, J.P., Goupil, M.J., *et al.*, 2015a, A&A, 579, A31
Belkacem, K., Marques, J.P., Goupil, M.J., *et al.*, 2015b, A&A, 579, A30
Belkacem, K., Samadi, R., Goupil, M.J., *et al.*, 2009, A&A, 494, 191
Belkacem, K., Samadi, R., Goupil, M.J., Kupka, F., & Baudin, F., 2006, A&A, 460, 183
Benomar, O., Belkacem, K., Bedding, T.R., *et al.*, 2014, ApJ, 781, L29
Buzasi, D., Catanzarite, J., Laher, R., *et al.*, 2000, ApJ, 532, L133
Cantiello, M., Mankovich, C., Bildsten, L., Christensen-Dalsgaard, J., & Paxton, B., 2014, ApJ, 788, 93
Ceillier, T., Eggenberger, P., García, R.A., & Mathis, S., 2013, A&A, 555, A54
Chaplin, W.J., Houdek, G., Elsworth, Y., *et al.*, 2005, MNRAS, 360, 859
Chaplin, W.J., & Miglio, A., 2013, ARA&A, 51, 353
Charbonnel, C., & Talon, S., 2005, Science, 309, 2189

- Christensen-Dalsgaard, J., 2004, *Sol. Phys.*, 220, 137
- Christensen-Dalsgaard, J., 2012, in *Astronomical Society of the Pacific Conference Series*, Vol. 462, *Progress in Solar/Stellar Physics with Helio- and Asteroseismology*, ed. H. Shibahashi, M. Takata, & A.E. Lynas-Gray, 503
- Christensen-Dalsgaard, J., & Frandsen, S., 1983, *Solar Phys.*, 82, 469
- Corsaro, E., Fröhlich, H.-E., Bonanno, A., *et al.*, 2013, *MNRAS*, 430, 2313
- De Ridder, J., Barban, C., Baudin, F., *et al.*, 2009, *Nature*, 459, 398
- Deheuvels, S., Ballot, J., Beck, P.G., *et al.*, 2015, *A&A*, 580, A96
- Deheuvels, S., Doğan, G., Goupil, M.J., *et al.*, 2014, *A&A*, 564, A27
- Deheuvels, S., García, R.A., Chaplin, W.J., *et al.*, 2012, *ApJ*, 756, 19
- Dupret, M.-A., Belkacem, K., Samadi, R., *et al.*, 2009, *A&A*, 506, 57
- Dziembowski, W.A., 1971, *Acta. Astron.*, 21, 289
- Dziembowski, W.A., Gough, D.O., Houdek, G., & Sienkiewicz, R., 2001, *MNRAS*, 328, 601
- EGgenberger, P., Lagarde, N., Miglio, A., *et al.*, 2017, *A&A*, 599, A18
- EGgenberger, P., Montalbán, J., & Miglio, A., 2012, *A&A*, 544, L4
- Fuller, J., LeCoanet, D., Cantiello, M., & Brown, B., 2014, *ApJ*, 796, 17
- Godart, M., Noels, A., Dupret, M.-A., & Lebreton, Y., 2009, *MNRAS*, 396, 1833
- Goupil, M.-J., 2011, **ArXiv e-prints**
- Goupil, M.J., Mosser, B., Marques, J.P., *et al.*, 2013, *A&A*, 549, A75
- Grigahcène, A., Dupret, M.-A., Gabriel, M., Garrido, R., & Scuflaire, R., 2005, *A&A*, 434, 1055
- Grosjean, M., Dupret, M.-A., Belkacem, K., *et al.*, 2014, **ArXiv e-prints**
- Grotsch-Noels, A. & Deheuvels, S., 2016, *IV.1 Insights on the internal structure of stars as provided by seismology*, ed. CoRot Team, 181
- Grundahl, F., Kjeldsen, H., Frandsen, S., *et al.*, 2006, *Mem. Soc. Astron. Italiana*, 77, 458
- Hekker, S., & Christensen-Dalsgaard, J., 2016, **ArXiv e-prints**
- Houdek, G., Balmforth, N.J., Christensen-Dalsgaard, J., & Gough, D.O., 1999, *A&A*, 351, 582
- Huber, D., Bedding, T.R., Stello, D., *et al.*, 2011, *ApJ*, 743, 143
- Kjeldsen, H., & Bedding, T.R., 1995, *A&A*, 293, 87
- Kjeldsen, H. & Bedding, T.R., 2011, *A&A*, 529, L8
- Lee, U., 2007, in *Astronomical Society of the Pacific Conference Series*, Vol. 361, *Active OB-Stars: Laboratories for Stellare and Circumstellar Physics*, ed. A.T. Okazaki, S.P. Owocki, & S. Stefl, 45
- Lee, U., Neiner, C., & Mathis, S., 2014, *MNRAS*, 443, 1515
- Lee, U. & Saio, H., 1993, *MNRAS*, 261, 415
- Libbrecht, K.G., 1988, *ApJ*, 334, 510
- Maeder, A., & Meynet, G., 2014, *ApJ*, 793, 123
- Marques, J.P., Goupil, M.J., Lebreton, Y., *et al.*, 2013, *A&A*, 549, A74
- Mosser, B., Barban, C., Montalbán, J., *et al.*, 2011, *A&A*, 532, A86
- Mosser, B., Belkacem, K., Pinçon, C., *et al.*, 2017, *A&A*, 598, A62

- Mosser, B., Benomar, O., Belkacem, K., *et al.*, 2014, *A&A*, 572, L5
- Mosser, B., Elsworth, Y., Hekker, S., *et al.*, 2012a, *A&A*, 537, A30
- Mosser, B., Goupil, M.J., Belkacem, K., *et al.*, 2012b, *A&A*, 548, A10
- Mosser, B., & Miglio, A., 2016, IV.2 Pulsating red giant stars, ed. CoRot Team, 197
- Mosser, B., Vradard, M., Belkacem, K., Deheuvels, S., & Goupil, M.J., 2015, *A&A*, 584, A50
- Ouazzani, R.-M., Goupil, M.J., Dupret, M.-A., & Marques, J.P., 2013, *A&A*, 554, A80
- Pinçon, C., Belkacem, K., & Goupil, M.J., 2016a, *A&A*, 588, A122
- Pinçon, C., Belkacem, K., & Goupil, M.J. 2016b, in SF2A-2016: Proceedings of the Annual meeting of the French Society of Astronomy and Astrophysics, ed. C. Reylé, J. Richard, L. Cambrésy, M. Deleuil, E. Pécontal, L. Tresse, & I. Vauglin, 179–183
- Press, W.H., 1981, *ApJ*, 245, 286
- Rauer, H., Catala, C., Aerts, C., *et al.*, 2014, *Exper. Astron.*, 38, 249
- Ricker, G.R., Winn, J.N., Vanderspek, R., *et al.*, 2015, *J. Astron. Telesc., Instrum. Syst.*, 1, 014003
- Rüdiger, G., Gellert, M., Spada, F., & Tereshin, I., 2015, *A&A*, 573, A80
- Samadi, R., 2011, in *Lecture Notes in Physics*, Berlin Springer Verlag, Vol. 832, Lecture Notes in Physics, Berlin Springer Verlag, ed. J.-P. Rozelot & C. Neiner, 305
- Samadi, R., Belkacem, K., Dupret, M.-A., *et al.*, 2012, *A&A*, 543, A120
- Samadi, R., Belkacem, K., & Sonoi, T., 2015, in *EAS Publications Series*, Vol. 73, EAS Publications Series, 111–191
- Samadi, R., Georgobiani, D., Trampedach, R., *et al.*, 2007, *A&A*, 463, 297
- Scuflaire, R., 1974, *A&A*, 36, 107
- Severino, G., Straus, T., & Steffen, M., 2008, *Sol. Phys.*, 251, 549
- Shibahashi, H., 1979a, *PASJ*, 31, 87
- Shibahashi, H., 1979b, *PASJ*, 31, 87
- Spada, F., Gellert, M., Arlt, R., & Deheuvels, S., 2016, *A&A*, 589, A23
- Spruit, H.C., 1999, *A&A*, 349, 189
- Spruit, H.C., 2002, *A&A*, 381, 923
- Tassoul, M., 1980, *ApJS*, 43, 469
- Townsend, R., 2014, in *IAU Symposium*, Vol. 301, *IAU Symposium*, ed. J.A. Guzik, W.J. Chaplin, G. Handler, & A. Pigulski, 153–160
- Townsend, R. & MacDonald, J., 2008, in *IAU Symposium*, Vol. 250, *IAU Symposium*, ed. F. Bresolin, P.A. Crowther, & J. Puls, 161–166
- Vradard, M., Mosser, B., & Samadi, R., 2016, *A&A*, 588, A87
- Zahn, J.-P., 1992, *A&A*, 265, 115